On Marangoni convective patterns driven by an exothermic chemical reaction in two-layer systems

D. A. Bratsun and A. De Wit
Service de Chimie Physique and Center for Nonlinear Phenomena and Complex Systems, CP 231, Université Libre de Bruxelles, 1050 Brussels, Belgium

(Received 28 May 2003; accepted 23 December 2003; published online 8 March 2004)

This article is devoted to the investigation of Marangoni-driven pattern formation at the interface between two immiscible fluids filling a Hele-Shaw cell, each of them containing a reactant of an exothermic neutralization reaction. In such a system, convective patterns arise when one reactant diffuses through the interface to react with the other chemical species in one of the fluids. A chemo-hydrodynamical pattern appears due to Marangoni instabilities taking place because of heat and solutal driven changes of the surface tension. The mathematical model we develop consists in a set of reaction-diffusion-advection equations ruling the evolution of concentrations and temperature coupled to Navier–Stokes equation, written in a Hele-Shaw approximation. In our analysis, the time-dependent convectionless reaction-diffusion base state is first obtained and studied in detail. Next, we perform a linear stability analysis of this base state with regard to thermal and solutal Marangoni effects to determine the parameter values beyond which convection occurs. Finally, we perform numerical simulations of the fully nonlinear system and study the influence of the different parameters on pattern formation. © *2004 American Institute of Physics.*
[DOI: 10.1063/1.1648641]

I. INTRODUCTION

In recent years binary liquid–liquid and gas–liquid systems with an interfacial chemical reaction have been the subject of increased fundamental investigations of the interaction between reaction-diffusion phenomena and pure hydrodynamic instabilities. In such systems, hydrodynamic instability of the fluid interface may generate local convective fluxes and thereby markedly affect the reaction as well as the interface heat and mass transfers. In these cases, self-organization processes may lead to a specific dissipation pattern formation of chemo-hydrodynamic nature.

The recent book by Nepomnyashchy, Velarde, and Colinet[1] provides a comprehensive bibliography for the studies devoted to all variety of interfacial phenomena. So, we skip in this review the numerous studies on pure heat and mass transfer processes occurring along or across an interface and focus our attention on such systems where a chemical reaction takes place.

Experimental evidence in liquid–liquid systems of interfacial convection exhibiting a high degree of ordering or interfacial turbulence, when mass transfer is accompanied by chemical reaction, has been reported in the literature for reactions of different types. Probably the first description of such phenomena is that of Quincke,[2] who observed spontaneous emulsification when a solution of lauric acid in oil is brought in contact with an aqueous solution of NaOH. More recently Sherwood and Wei[3] observed spontaneous turbulence in the extraction of acetic acid from an organic solvent into an alkaline solution and acceleration of the interfacial reaction by convection. Dupeyrat and Nakache[4–6] also observed interfacial turbulence related to the reaction of an alkyl ammonium ion with picric acid at an oil–aqueous interface.

Another example of spontaneous turbulence at the interface was found in the area of nuclear fuel reprocessing. Thomson *et al.* observed interfacial instabilities during the extraction of uranyl nitrate from its nitric acid solution.[7] One more example was given by Avnir and Kagan who have studied pattern formation at liquid–gas interfaces driven by photochemical reactions.[8] Kai *et al.*[9] have studied the dynamics of chemically driven nonlinear waves and oscillations at an oil–water interface.

Very recently, new phenomena attributed to heat and solutal effects due to an exothermic neutralization reaction interplaying with a liquid–liquid interface and convection was observed experimentally by Eckert and Grahn.[10] These authors reported about a novel instability occurring when an organic solution containing an acid is in contact with an aqueous solution in which NaOH is dissolved. Resulting self-sustained dynamics and pattern formation in the form of plumes and fingers were suggested to originate from the coupling between different hydrodynamic instabilities, such as boundary layer and double diffusion instabilities. An impressive regular structure in the form of long self-growing cells with one side keeping contact with the interface and the other side propagating in the direction out of the interface is observed in the same system when NaOH is replaced by an organic base.[11] In these recent experiments, several mechanisms of instability (surface tension driven or buoyancy driven ones) may compete. The use of an organic base instead of NaOH allows for possible increased influence of Marangoni effects as the salt formed is of increased chain length. It is the purpose of this article to investigate to what

extent Marangoni effects alone are sufficient to drive any instability in such chemo-hydrodynamic pattern formation. If a Marangoni mechanism turns out to be possible, we aim also to understand which effect, thermal or solutal, is most important for the system.

To finish the review of experimental study, let us mention one more recent work. Ermakov *et al.*[12] have used a system similar to that of Eckert *et al.*, concentrating their attention on measuring changes in the kinetic laws of mass transfer in the system.

Numerous theoretical studies concerned with the effect of chemical reaction on interfacial instability have focused for the most part on the linear analysis of conditions under which the instability develops. Ruckenstein and Berbente[13] were the first to conduct such an analysis. They studied the stability of a two-phase system where a first-order reaction is taking place in one of the phases and found that no general criteria, which would be similar to that earlier derived by Sternling and Scriven[14] for a nonreactive two-layer system with a single solute diffusing from one layer to another, could be established because each particular type of reaction requires a separate consideration for the derivation of interfacial stability criteria. The effect on the system's stability of different types of reactions, which occur solely on the interface, was analyzed in the papers of Steinchen and Sanfeld[15,16] and Hennenberg *et al.*[17] They concluded that a chemical instability due to an interfacial reaction can induce a mechanical instability and vice versa. A similar approach was applied by Mendez-Tatsis and Perez De Ortiz to a liquid–liquid system with a reversible interfacial reaction occurring in some metal extraction processes.[18] Let us also mention one more recent study by Texier-Picard, Pojman, and Volpert[19] devoted to the investigation of polymerization fronts converting a liquid monomer into liquid polymer assumed as immiscible. They were interested to study the influence of interfacial tension on the front stability taking into account the exothermicity of the polymerization reaction.

The nonlinear aspects of the effect of chemical reactions on the development of interfacial convection and mass transfer have yet received little attention. Among the nonlinear studies a series of papers by Buyevich *et al.*[20,21] investigated the conditions of appearance and nonlinear development of concentrational capillary instability at the interface between two liquids in the presence of an interfacial reaction of second order. The Marangoni instability driven by chemical reactions in systems with liquid–liquid interface has been studied not only in layer geometries. Velarde[22] gives a wide review of the results on Marangoni instability occurring when a liquid drop is immersed in another immiscible liquid. In this case the instability induced by chemical reactions leads to self-propelled drop motion, overcoming viscous drag. It is also worthy to mention two recent papers which, though do not deal with chemical reactions, study the effect of strong heat generation occurring at the interface. In the first of them, Skurygin and Dilman[23] perform a linear stability analysis of a gas–liquid interface during the combined process of desorption and evaporation. In the second paper, Nepomnyashchy and Simanovskii[24] carry out numerical simulation of finite-amplitude convective regimes for a two-liquid system with joint action of external heating and heat sources distributed on the interface between layers. The latter model some aspects of exothermal chemical reactions occurring on the interface.

In the majority of these articles, the chemical reaction is assumed interfacial, i.e., taking place solely on the interface. As we shall show here, the possibility for chemical species to diffuse and react in the bulk of one of the fluids leads immediately to a new kind of instability driven by the joint action of exothermic chemical reaction, diffusion processes and dependence of surface tension on heat and mass gradients.

The purpose of the present work is to focus on the particular role of Marangoni instabilities in chemo-convective patterns as experimentally observed in Refs. 10, 11. On Earth, Marangoni effects are difficult to separate from other sources of instability such as buoyancy driven Rayleigh–Taylor, Rayleigh–Bénard or double diffusive mechanisms. It is therefore important to understand each of these instabilities and their respective coupling with chemical reactions separately. Pure Marangoni effects should be observed in Hele-Shaw cells oriented horizontally with regard to gravity or ideally in zero-gravity conditions. In this article, we analyze the coupling between a simple exothermic neutralization reaction with pure Marangoni driven convection in a setup similar to that experimentally analyzed by Eckert *et al.*[10,11] assuming that gravity does not play any role. We investigate the coupling between the chemical reactions and hydrodynamics both by linear stability analysis and nonlinear simulations.

The paper is organized as follows: in Sec. II we formulate the problem and discuss all aspects of the proposed mathematical model. In Sec. III we obtain the reaction-diffusion base state and, then, apply the linear analysis to study its stability wit regard to convection in Sec. IV. The details of the numerical method and numerical results are given in Sec. V. Section VI summarizes the results and provides some discussion.

II. THEORETICAL MODEL

We consider a two-layer system consisting of two immiscible incompressible liquid solvents, separated by a plain and nondeformable interface with pinning contact lines, and confined by two vertical parallel solid plates (see Fig. 1). We assume that carboxylic acid A dissolved in the upper organic solvent (such as cyclohexane), diffuses through the interface to react with a base B, dissolved in the lower aqueous layer to form a salt under the production of water. Such a neutralization reaction can be described by the simplified equation: $A+B\rightarrow S$, where S denotes the salt. This reaction is accompanied by heat release Q and takes place solely in the lower aqueous phase as the base is immiscible in the upper organic phase. The rate of reaction is characterized by the reaction rate constant K.

We assume further that the gap-width $2d$ between the plates is much smaller than their lateral extension which leads us to use a Hele-Shaw approximation for velocity and temperature fields, i.e., we assume that they follow a parabolic profile along the gap:

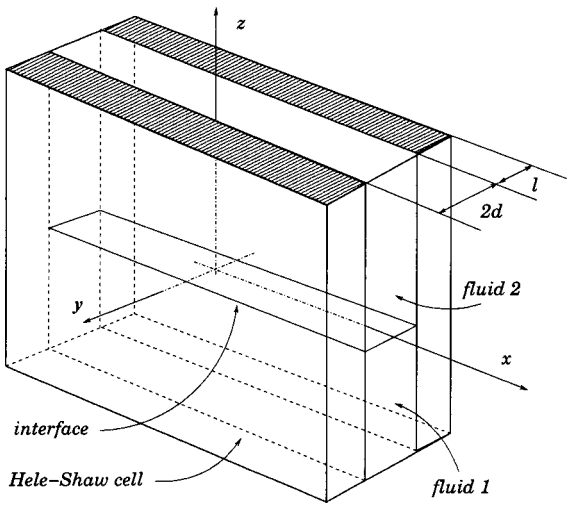

FIG. 1. Geometrical configuration of the two-layer system and coordinate axes.

$$\mathbf{u}_i(x,y,z)=\frac{3}{2}\left(1-\frac{y^2}{d^2}\right)\mathbf{v}_i(x,z),$$
$$\Theta_i(x,y,z)=\frac{3}{2}\frac{\mathrm{Bi}}{(3+\mathrm{Bi})}\left(\frac{2}{\mathrm{Bi}}+1-\frac{y^2}{d^2}\right)T_i(x,z), \tag{1}$$

satisfying the boundary conditions at the solid plates:

$$\mathbf{u}=0, \quad \frac{\partial\Theta_i}{\partial(y/d)}\pm\mathrm{Bi}(\Theta_i-\Theta_0)=0 \quad \text{for } y=\pm d, \tag{2}$$

where $\mathbf{u}_i(u_x,u_y,u_z)$ and $\mathbf{v}_i(v_x,v_z)$ are the three- and two-component vector fields, respectively, Θ_i and T_i are temperature fields before and after the procedure of averaging, respectively. The reference temperature Θ_0 is room temperature, and indexes $i=1,2$ refer to the lower ($z<0$) and upper ($z>0$) layer, respectively. The dimensionless Biot number Bi, is defined as $\mathrm{Bi}=d\gamma_T/\kappa_1$, where γ_T is the heat exchange coefficient between the fluid and the solid walls and κ_1 is the coefficient of thermal conductivity of water in the lower layer. Depending on the plates composition and thickness l, the Biot number Bi may take a value from 0 (thermo-isolated plates) to ∞ (highly conductive plates).

Evolution equations in the Hele-Shaw approximation are obtained by inserting (1) into the standard three-dimensional Navier–Stokes equations coupled to heat and reaction-diffusion equations, and averaging with respect to the y-space direction perpendicular to the solid plates.[25] This procedure reduces the system geometry to two semi-infinite two-dimensional regions filled by two fluids and separated by a line $z=0$. In the absence of gravity, the governing equations take the following form:

$$\nabla\cdot\mathbf{v}_i=0,$$

$$\frac{\partial\mathbf{v}_i}{\partial t}+\frac{6}{5}\mathbf{v}_i\cdot\nabla\mathbf{v}_i=-\frac{1}{\rho_i}\nabla p_i+\nu_i\Delta\mathbf{v}_i-3\frac{\nu_i}{d^2}\mathbf{v}_i,$$

$$\frac{\partial T_i}{\partial t}+\frac{3}{5}\frac{(5+2\mathrm{Bi})}{(3+\mathrm{Bi})}\mathbf{v}_i\cdot\nabla T_i=\chi_i\Delta T_i-\frac{\chi_i}{d^2}\frac{3\mathrm{Bi}}{(3+\mathrm{Bi})}T_i-\delta_i K\frac{Q}{c_{pi}\rho_i}A_iB,$$
$$\frac{\partial A_i}{\partial t}+\mathbf{v}_i\cdot\nabla A_i=D_{Ai}\Delta A_i-\delta_i KA_iB, \quad i=1,2, \tag{3}$$
$$\frac{\partial B}{\partial t}+\mathbf{v}_1\cdot\nabla B=D_B\Delta B-KA_1B,$$
$$\frac{\partial S}{\partial t}+\mathbf{v}_1\cdot\nabla S=D_S\Delta S+KA_1B,$$

where p_i is the pressure, A_i, B, and S are acid, base, and salt concentrations, respectively. The parameter δ_i takes the values $\delta_1=1$, $\delta_2=0$ implying that the reaction takes place solely in the lower layer. The densities, dynamic, and kinematic viscosities, heat conductivities, temperature diffusivities, diffusivities of acid, base and salt are, respectively, equal to ρ_i, η_i, ν_i, κ_i, χ_i, D_{Ai}, D_B, D_S. The boundary conditions are

$$z\to-\infty: \ \mathbf{v}_1=0, \quad T_1=0, \quad A_1=0, \quad B=B_0, \quad S=0,$$
$$z\to+\infty: \ \mathbf{v}_2=0, \quad T_2=0, \quad A_2=A_0,$$
$$z=0: \ \mathbf{v}_1=\mathbf{v}_2, \quad T_1=T_2, \quad A_1=A_2,$$
$$\kappa_1\frac{\partial T_1}{\partial z}=\kappa_2\frac{\partial T_2}{\partial z}, \quad D_{A1}\frac{\partial A_1}{\partial z}=D_{A2}\frac{\partial A_2}{\partial z},$$
$$\frac{\partial B}{\partial z}=0, \quad \frac{\partial S}{\partial z}=0,$$
$$\frac{\partial\sigma}{\partial x}=\eta_1\frac{\partial v_{x1}}{\partial z}-\eta_2\frac{\partial v_{x2}}{\partial z},$$
$$\sigma=\sigma_0-\sigma_T T-\sigma_A A-\sigma_S S,$$

where A_0 and B_0 are the initial concentration of acid and base and σ is the surface tension.

Let us outline explicitly the assumptions we make:

(1) The gap between the vertical plates is small enough so that the fluid flow may be considered as quasi-two-dimensional.
(2) The concentrations of chemical species A, B, and S are small enough so that the properties of the fluid are independent on concentration.
(3) The three chemical species have the same diffusion coefficient, i.e., $D_B=D_S=D_{A1}$ in the aqueous phase.
(4) The acid-partition ratio is assumed to be equal to unity.
(5) The effects of baro- and thermo-diffusion (such as the Soret effect) are negligible.
(6) The base B and salt S do not dissolve in the upper layer.
(7) The base does not produce any surface effect, which is motivated by experimental observations.[11]
(8) The surface tension σ depends linearly on the temperature and concentrations of acid and salt.
(9) Surface tension is presumed to be high enough to render the interface surface resistant to any deformation.

(10) The contact lines of the interface are assumed to be pinned, i.e., they are unable to move.

To nondimensionalize the problem, we assume that chemical and diffusion processes occur on the same time scale. We choose therefore the following characteristic scales: for time $\tau_R = 1/KA_0$, for length $h = \sqrt{D_{A1}\tau_R}$, for velocity $\sqrt{D_{A1}/\tau_R}$, for pressure $3\rho_1\nu_1 D_{A1}/d^2$, for concentrations A_0, for temperature $QD_{A1}A_0/\kappa_1$ and obtain the dimensionless equations for the lower layer,

$$\nabla \cdot \mathbf{v}_1 = 0, \tag{4}$$

$$\frac{\epsilon}{\mathrm{Sc}}\left(\frac{\partial \mathbf{v}_1}{\partial t} + \frac{6}{5}\mathbf{v}_1 \cdot \nabla \mathbf{v}_1\right) = -\nabla p_1 + \epsilon \Delta \mathbf{v}_1 - \mathbf{v}_1, \tag{5}$$

$$\frac{\epsilon}{\mathrm{Le}}\left(\frac{\partial T_1}{\partial t} + \frac{3}{5}\frac{(5+2\mathrm{Bi})}{(3+\mathrm{Bi})}\mathbf{v}_1 \cdot \nabla T_1\right) = \epsilon \Delta T_1 - \frac{\mathrm{Bi}}{(3+\mathrm{Bi})}T_1 + \epsilon A_1 B, \tag{6}$$

$$\frac{\partial A_1}{\partial t} + \mathbf{v}_1 \cdot \nabla A_1 = \Delta A_1 - A_1 B, \tag{7}$$

$$\frac{\partial B}{\partial t} + \mathbf{v}_1 \cdot \nabla B = \Delta B - A_1 B, \tag{8}$$

$$\frac{\partial S}{\partial t} + \mathbf{v}_1 \cdot \nabla S = \Delta S + A_1 B, \tag{9}$$

for the upper layer:

$$\nabla \cdot \mathbf{v}_2 = 0, \tag{10}$$

$$\frac{\epsilon}{\mathrm{Sc}}\left(\frac{\partial \mathbf{v}_2}{\partial t} + \frac{6}{5}\mathbf{v}_2 \cdot \nabla \mathbf{v}_2\right) = -\frac{1}{\rho}\nabla p_2 + \nu\epsilon \Delta \mathbf{v}_2 - \nu \mathbf{v}_2, \tag{11}$$

$$\frac{\epsilon}{\mathrm{Le}}\left(\frac{\partial T_2}{\partial t} + \frac{3}{5}\frac{(5+2\mathrm{Bi})}{(3+\mathrm{Bi})}\mathbf{v}_2 \cdot \nabla T_2\right) = \chi\epsilon \Delta T_2 - \chi\frac{\mathrm{Bi}}{(3+\mathrm{Bi})}T_2, \tag{12}$$

$$\frac{\partial A_2}{\partial t} + \mathbf{v}_2 \cdot \nabla A_2 = D \Delta A_2, \tag{13}$$

with boundary conditions:

$$z \to -\infty: \quad \mathbf{v}_1 = 0, \quad T_1 = 0, \quad A_1 = 0, \quad B = \frac{1}{\gamma}, \quad S = 0, \tag{14}$$

$$z \to +\infty: \quad \mathbf{v}_2 = 0, \quad T_2 = 0, \quad A_2 = 1, \tag{15}$$

$$z = 0: \quad v_{z1} = v_{z2} = 0, \quad v_{x1} = v_{x2}, \quad T_1 = T_2, \quad A_1 = A_2, \tag{16}$$

$$\frac{\partial T_1}{\partial z} = \kappa \frac{\partial T_2}{\partial z}, \quad \frac{\partial A_1}{\partial z} = D\frac{\partial A_2}{\partial z}, \quad \frac{\partial B}{\partial z} = 0, \quad \frac{\partial S}{\partial z} = 0, \tag{17}$$

$$\frac{\partial v_{x1}}{\partial z} = \eta \frac{\partial v_{x2}}{\partial z} - M\frac{\partial T_1}{\partial x} - M_A\frac{\partial A_1}{\partial x} - M_S\frac{\partial S}{\partial x}. \tag{18}$$

TABLE I. List of dimensionless parameters.

$\epsilon = d^2/3h^2$	Aspect ratio of gap-width to scale of convective pattern
$\mathrm{Sc} = \nu_1/D_{A1}$	Schmidt number
$\mathrm{Le} = \chi_1/D_{A1}$	Lewis number
$M = \sigma_T A_0 \lvert Q \rvert h/\kappa_1\eta_1$	Thermal Marangoni number
$M_A = \sigma_A A_0 h/D_{A1}\eta_1$	Solutal Marangoni number related to acid
$M_S = \sigma_S A_0 h/D_{A1}\eta_1$	Solutal Marangoni number related to salt
$\mathrm{Bi} = d\gamma_T/\kappa_1$	Biot number
$\rho = \rho_2/\rho_1$	Density ratio
$\kappa = \kappa_2/\kappa_1$	Heat conductivity ratio
$\chi = \chi_2/\chi_1$	Heat diffusivity ratio
$\nu = \nu_2/\nu_1$	Kinematic viscosity ratio
$\eta = \eta_2/\eta_1$	Dynamic viscosity ratio
$D = D_{A2}/D_{A1}$	Acid diffusivity ratio
$\gamma = A_0/B_0$	Initial concentration ratio

The full list of dimensionless parameters, which appear in Eqs. (5)–(18), is given in Table I. Let us discuss the equations we obtain in more detail. First of all, let us note that in the experiments,[10] the Schmidt number is $\mathrm{Sc} \approx 900$ while the Lewis number is $\mathrm{Le} \approx 100$, which allows us to neglect the left-hand side of (5)–(6) and (11)–(12). It means that hydrodynamic and heat processes are here quick compared to reaction-diffusion processes.

Equations (5) and (11) differ from the two-dimensional Navier–Stokes equations by the additional dissipative terms proportional to velocities $\mathbf{v}_1$ and $\mathbf{v}_2$, respectively. These terms may be interpreted as the average friction force due to the presence of the plates and are analogous to Darcy term arising in equations for fluid filtration in porous medium. If the parameter ϵ is small enough, the Stokes term in (5) can be neglected and we recover Darcy's law. In fact $\epsilon = d^2/3h^2$ compares the gap-width $2d$ of the Hele-Shaw cell to the characteristic length scale $h = \sqrt{D_{A1}/KA_0}$ of the chemo-hydrodynamic pattern. Experimentally, convective patterns appearing at early times have a length scale roughly 2–3 times the gap-width $2d$. This gives a value $\epsilon \sim 0.1$ showing that diffusion of velocity and temperature should be taken into account. As a matter of fact, the presence of such Stokes second-order term is crucial, because the thermocapillary flow is driven by shear stresses and can therefore in general not be potential.[26] Thus, in all our calculations we keep the value $\epsilon = 0.1$. The specific choice of $\epsilon = 0.1$ results from the fact that diffusion and reactive processes are assumed here to occur on the same time scale, i.e., the ratio between the chemical time $\tau_R = 1/KA_0$ and the diffusive time $\tau_{\mathrm{diff}} = h^2/D_{A1} = (\sqrt{D_{A1}\tau_R})^2/D_{A1}$ is chosen to be equal to one. This assumption is made because the kinetic constant K is not known. In this way we decrease the number of dimensionless parameters to concentrate on parameters which can be changed during the experiment such as γ and the Marangoni numbers which can all be tuned by varying the concentrations.

Similarly to motion equations, heat equations (6) and (12) differ from standard two-dimensional heat equations by the additional Darcy-type term $\mathrm{Bi}\,T/(3+\mathrm{Bi})$. This term relates to the process of dissipation of heat through the solid plates. The difference with the Darcy term discussed above is that this term vanishes if the plates are made from thermo-

isolated material for which Bi=0. If the plates are highly conductive, the dissipation rate is maximal and Bi=∞. Let us estimate the Biot number for the experimental setup used in Ref. 10. The heat exchange coefficient γ_T may be estimated as $\gamma_T \approx \kappa_s / l$, where κ_s is the thermal conductivity of the solid plates and l is their thickness (Fig. 1). Taking into account that $l \approx d$ and that plates are made of glass, the conductivity of which is close to the conductivity of water filling the lower layer where the reaction occurs, we obtain Bi~1, which means that heat dissipation during the experiment is quite intensive. For the sake of generality, we consider two limiting cases: Bi=0 and Bi=∞.

As the diffusivity of the base is supposed to be equal to that of the salt $D_B = D_S$, we can derive an important relation reflecting a conservation law for species concentrations. By adding Eqs. (8) and (9) and taking into account the boundary conditions we obtain

$$B + S = \frac{1}{\gamma}, \tag{19}$$

which is used when the system is studied numerically.

By taking these notes into account, we can reduce the system of Eqs. (5)–(13) to the following form:

$$\begin{aligned}
&\Delta^2 \Psi_1 - \frac{1}{\epsilon}\Delta\Psi_1 = 0, \quad \Delta^2 \Psi_2 - \frac{1}{\epsilon}\Delta\Psi_2 = 0,\\
&\Delta T_1 - \frac{1}{\epsilon}\frac{\mathrm{Bi}}{(3+\mathrm{Bi})} T_1 = -A_1 B,\\
&\Delta T_2 - \frac{1}{\epsilon}\frac{\mathrm{Bi}}{(3+\mathrm{Bi})} T_2 = 0,\\
&\frac{\partial A_2}{\partial t} + \frac{\partial(\Psi_2, A_2)}{\partial(z,x)} = D\Delta A_2,\\
&\frac{\partial A_1}{\partial t} + \frac{\partial(\Psi_1, A_1)}{\partial(z,x)} = \Delta A_1 - A_1 B,\\
&\frac{\partial B}{\partial t} + \frac{\partial(\Psi_1, B)}{\partial(z,x)} = \Delta B - A_1 B,\\
&\frac{\partial S}{\partial t} + \frac{\partial(\Psi_1, S)}{\partial(z,x)} = \Delta S + A_1 B,
\end{aligned} \tag{20}$$

where

$$\frac{\partial(a,b)}{\partial(z,x)} = \frac{\partial a}{\partial z}\frac{\partial b}{\partial x} - \frac{\partial a}{\partial x}\frac{\partial b}{\partial z},$$

and with boundary conditions:

$$\begin{aligned}
&z \to -\infty: \quad \Psi_1 = 0, \quad \frac{\partial \Psi_1}{\partial z} = 0, \quad T_1 = 0, \quad A_1 = 0,\\
&B = \frac{1}{\gamma}, \quad S = 0;\\
&z \to +\infty: \quad \Psi_2 = 0, \quad \frac{\partial \Psi_2}{\partial z} = 0, \quad T_2 = 0, \quad A_2 = 1;\\
&z = 0: \quad \Psi_1 = \Psi_2 = 0, \quad \frac{\partial \Psi_1}{\partial z} = \frac{\partial \Psi_2}{\partial z},\\
&\frac{\partial^2 \Psi_1}{\partial z^2} = \eta\frac{\partial^2 \Psi_2}{\partial z^2} - M\frac{\partial T_1}{\partial x} - M_A\frac{\partial A_1}{\partial x} - M_S\frac{\partial S}{\partial x},\\
&T_1 = T_2, \quad \frac{\partial T_1}{\partial z} = \kappa\frac{\partial T_2}{\partial z}, \quad A_1 = A_2,\\
&\frac{\partial A_1}{\partial z} = D\frac{\partial A_2}{\partial z}, \quad \frac{\partial B}{\partial z} = 0, \quad \frac{\partial S}{\partial z} = 0,
\end{aligned}$$

where the stream function Ψ is defined as

$$v_x = \frac{\partial \Psi}{\partial z}, \quad v_z = -\frac{\partial \Psi}{\partial x}.$$

To conclude the discussion of the proposed model, let us enumerate the parameters which we keep constant in all our calculations and the values of which are inspired by the experiments:[10,11] $\eta = 0.4996$, $\kappa = 0.2482$, $D = 2.807$, and $\epsilon = 0.1$.

III. BASE STATE

In a first step we analyze the one-dimensional reaction-diffusion base state of the system assuming that there is no fluid flow. In that case, we look for the base state $(A_i^0(t,z), B^0(t,z), S^0(t,z), T_i^0(t,z))$ solution of (20) with $\Psi_i = 0$, which satisfies the following set of equations:

$$\begin{aligned}
&\frac{\partial^2 T_1^0}{\partial z^2} - \frac{1}{\epsilon}\frac{\mathrm{Bi}}{(3+\mathrm{Bi})} T_1^0 = -A_1^0 B^0,\\
&\frac{\partial^2 T_2^0}{\partial z^2} - \frac{1}{\epsilon}\frac{\mathrm{Bi}}{(3+\mathrm{Bi})} T_2^0 = 0,\\
&\frac{\partial A_1^0}{\partial t} = \frac{\partial^2 A_1^0}{\partial z^2} - A_1^0 B^0, \quad \frac{\partial A_2^0}{\partial t} = D\frac{\partial^2 A_2^0}{\partial z^2},\\
&\frac{\partial B^0}{\partial t} = \frac{\partial^2 B^0}{\partial z^2} - A_1^0 B^0, \quad \frac{\partial S^0}{\partial t} = \frac{\partial^2 S^0}{\partial z^2} + A_1^0 B^0,
\end{aligned} \tag{21}$$

and boundary conditions

$$\begin{aligned}
&z \to -\infty: \quad T_1^0 = 0, \quad A_1^0 = 0, \quad B^0 = \frac{1}{\gamma}, \quad S^0 = 0,\\
&z \to +\infty: \quad T_2^0 = 0, \quad A_2^0 = 1,\\
&z = 0: \quad T_1^0 = T_2^0, \quad \frac{\partial T_1^0}{\partial z} = \frac{\partial T_2^0}{\partial z}\kappa, \quad A_1^0 = A_2^0,\\
&\frac{\partial A_1^0}{\partial z} = D\frac{\partial A_2^0}{\partial z}, \quad \frac{\partial B^0}{\partial z} = 0, \quad \frac{\partial S^0}{\partial z} = 0.
\end{aligned}$$

Because of the quadratic nonlinearity in the chemical kinetics, no analytic solution can be obtained for the reaction-diffusion state, and the system is studied numerically. The

important relation $B^0+S^0=1/\gamma$ holds, which helps to simplify calculations. In order to integrate system (20) with $\Psi=0$, we use an explicit finite-difference method (see Sec. V). Instead of the boundary conditions at infinity in (20), the simulations are done in the finite range $-L<z<L$, where L is varied from 1 to 10 to be sure that the obtained results are independent of L.

As we want to investigate the influence of the reactions on the hydrodynamical Marangoni instability, it is most natural to analyze the effect of the parameter γ, the ratio between initial acid and base concentration A_0/B_0. Two important cases that manifest different dynamics are considered: the case $\gamma\leqslant 1$, for which the initial concentration of acid is smaller or equal to that of the base, and the case $\gamma>1$, for which the acid concentration is in excess. As we shall see, the resulting dynamics are strongly affected by γ as, for $\gamma\leqslant 1$, the reaction front remains located near the interface and is practically steady while, for $\gamma>1$, the reaction front moves away from the interface. Let us examine these two situations considering successively the cases $\gamma=1$ and $\gamma=10$.

A. Quasisteady reaction front: $\gamma=1$

The base state profiles for the concentrations and temperature as a function of time are presented in Figs. 2(a) and 2(b), respectively, in the case of highly conductive walls (Bi $=\infty$). Profiles are plotted with time interval $\Delta t=1$, starting from $t=0$ up to $t=14$. As we see in Fig. 2(a), in the case where initial concentrations of acid and base are equal ($\gamma=1$), the dynamics of acid in the lower reactive layer tends to some quasisteady state reflecting the balance between consumption of the reactant and its supply from the upper layer. In contrast to that, the concentrations of base and salt change quickly: the base concentration decreases, while the salt concentration increases as $S^0=1/\gamma-B^0$. While concentration profiles look like expected, the temperature profiles shown in Fig. 2(b) have a remarkable feature, i.e., the presence of a maximum located below the interface. The existence of this maximum in the bulk can be evidenced not only numerically, but also analytically. Indeed, the temperature profile $T_2^0(t,z)$ in the upper layer can be readily derived:

$$T_2^0(t,z)=\xi(t)\exp\left(-\frac{\mathrm{Bi}}{3+\mathrm{Bi}}\frac{z}{\sqrt{\epsilon}}\right),$$

where $\xi(t)$ denotes the temperature at the interface. The temperature gradient at the interface in the lower layer can then be written as $\partial T_1^0/\partial z|_{z=0}=-\kappa\,\mathrm{Bi}\,\xi(t)/\sqrt{\epsilon}(3+\mathrm{Bi})$, i.e., it is always negative (excepting the case of perfect thermal insulators Bi=0), which means that the temperature must feature a maximum between the interface and $z\to-\infty$, where $T=0$. The time-dependent dynamics of this gradient is shown in the inset of Fig. 2(b). As we see, the absolute value of the gradient first grows from zero at $t=0$ to its maximum at about $t=0.5$, and then decreases slowly in time. A similar behavior is followed by the temperature profile itself. This result could have been anticipated if we are reminded that no reaction occurs in the upper layer. It means that the heat produced by the reaction must diffuse into the upper layer causing heat loss in the domain close to the interface. The final balance between diffusion of heat through the interface, diffusion of heat through the solid plates (dissipation), and generation of heat by the reaction leads to the temperature maximum located below the interface. This temperature maximum corresponds to the front of reaction. As we see from Fig. 2(b), in the case $\gamma=1$, the reaction front tends to a steady position when $t>0.5$.

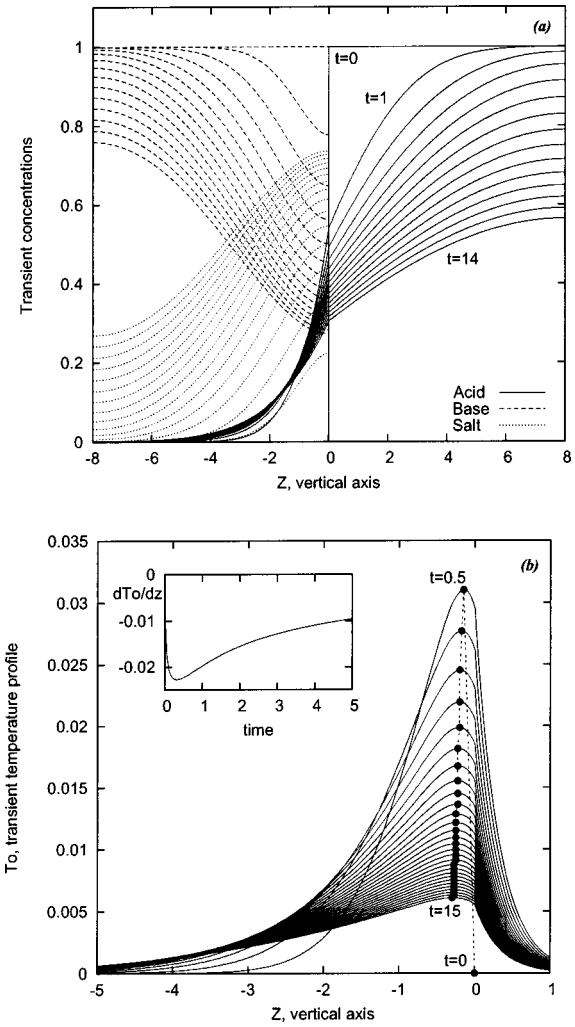

FIG. 2. Base state profiles for concentrations (a) and temperature (b) for $\gamma=1$. The inset in (b) shows the time-dependent dynamics of the temperature gradient at the interface in the lower layer.

The case Bi=0 is singular if one assume simultaneously the infinite range $-\infty<z<\infty$ and immediate response of the heat field to any disturbances in the system ($\partial T/\partial t=0$). In the numerical simulation, when the finite geometry was considered, this singularity disappeared and we observed the formation of the temperature maximum in the lower layer, too.

The existence of a temperature maximum at a given distance below the interface is a key ingredient to get an instability of Marangoni-type. Indeed, let us imagine that a hot spot appears spontaneously at the interface between the fluids. Then the resulting surface tension gradient will induce a fluid movement along the interface directed out of the spot. In this case, the element of fluid rising towards the interface from the bulk makes the spot hotter giving rise to the instability.

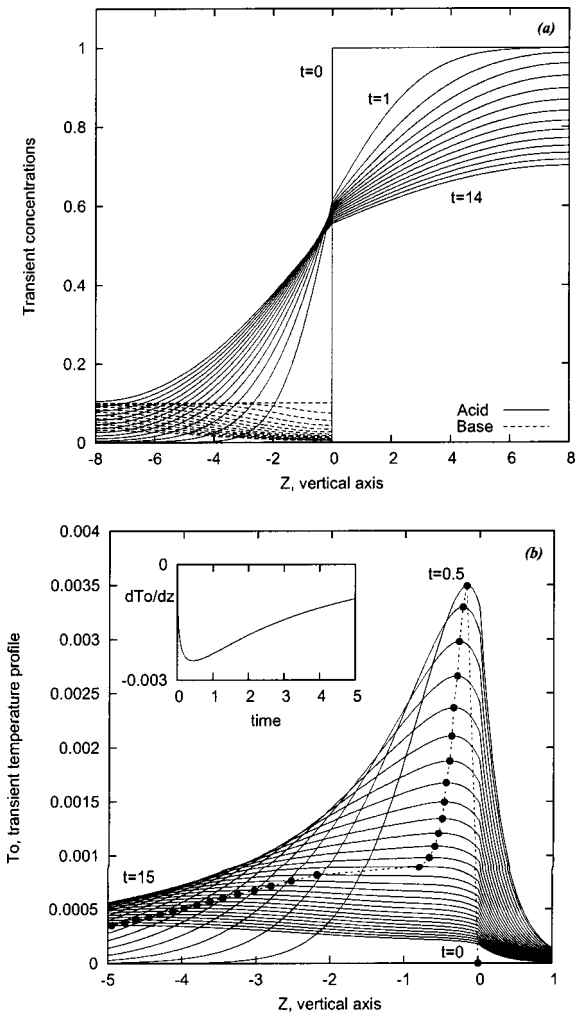

FIG. 3. Base state profiles for concentrations (a) and temperature (b) for $\gamma=10$. The inset in (b) is as in Fig. 2(b).

B. Moving reaction front: $\gamma=10$

The profile dynamics for concentrations and temperature for the case $\gamma=10$ are presented in Figs. 3(a) and 3(b), respectively. We see that the behavior of the system has changed qualitatively. When the initial concentration of acid is higher than that of the base, the acid profile in the lower layer is no more quasisteady as before: the acid does not meet enough base to react and diffuses quickly far away of the interface inducing a movement of the reaction front in the same direction. The front movement manifests itself in the movement of the temperature maximum shown in Fig. 3(b).

To summarize, two different base states are observed in the system depending whether the acid is in excess or not. As shown in Fig. 4, the reaction front corresponding to a temperature maximum remains stationary close to the interface up to a critical value of the order of $\gamma_{cr}\sim 2$. Beyond this value, the temperature maximum moves away of the interface after an initial transient.

The same phenomenon is observed experimentally,[11] i.e., both traveling and quasistanding reaction front are observed depending on the initial concentrations of acid and base.

In the conclusion of this section, we note that the movement of the temperature maximum implies a possible dynamic change of the wavelength of the convection pattern in time. The importance of the two different reaction-diffusion base states for the stability properties of the system will be made clear in the next section.

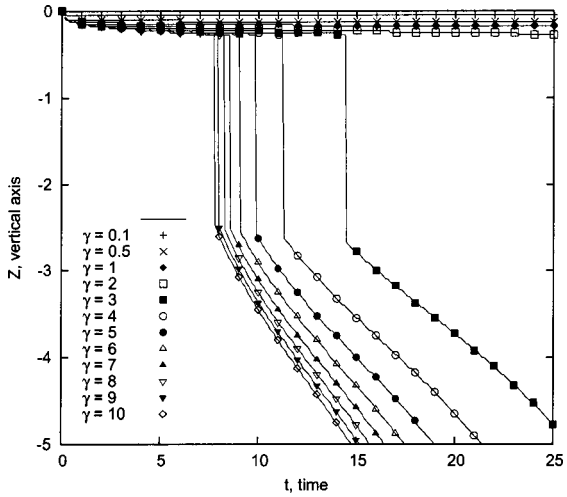

FIG. 4. Time-dependent dynamics of the temperature maximum shown for different values of γ.

IV. LINEAR STABILITY ANALYSIS

A. Equations and solution method

The next step in our analysis involves finding the conditions under which the reaction-diffusion solution loses stability to give rise to convective solutions. To do so, we analyze the stability of the base state by linearizing the original system of Eqs. (20) around the base state $(A_i^0(t,z),B^0(t,z),S^0(t,z),T_i^0(t,z))$ determined in the previous section. First, we assume that small, monotonic disturbances periodic in the x-direction are superimposed upon the base state (21) in the following manner:

$$\begin{pmatrix} \Psi_i(t,x,z) \\ T_i(t,x,z) \\ A_i(t,x,z) \\ B(t,x,z) \\ S(t,x,z) \end{pmatrix} = \begin{pmatrix} 0 \\ T_i^0(t,z) \\ A_i^0(t,z) \\ B^0(t,z) \\ S^0(t,z) \end{pmatrix} + \begin{pmatrix} \varphi_i(t,z) \\ \vartheta_i(t,z) \\ a_i(t,z) \\ b(t,z) \\ s(t,z) \end{pmatrix} e^{Ikx}, \quad i=1,2 \tag{22}$$

where φ_i, ϑ_i, a_i, b, s are the amplitude of the disturbances of the stream function, temperature, acid, base, and salt concentrations, respectively, while k is their wave number.

The linearized equations governing the evolution of disturbances are derived by introducing (22) into Eqs. (20) and neglecting nonlinear terms. We get the following eigenvalue problem:

$$\Delta^2\varphi_1-\frac{1}{\epsilon}\Delta\varphi_1=0, \quad \Delta^2\varphi_2-\frac{1}{\epsilon}\Delta\varphi_2=0,$$

$$\Delta\vartheta_1-\frac{1}{\epsilon}\frac{\mathrm{Bi}}{(3+\mathrm{Bi})}\vartheta_1=-A_1^0(z,t)b-B^0(z,t)a_1,$$

$$\Delta\vartheta_2-\frac{1}{\epsilon}\frac{\mathrm{Bi}}{(3+\mathrm{Bi})}\vartheta_2=0,$$

$$\frac{\partial a_1}{\partial t}=\Delta a_1-A_1^0(z,t)b-B^0(z,t)a_1-\varphi_1'\frac{\partial A_1^0(z,t)}{\partial z},$$

$$\frac{\partial a_2}{\partial t}=D\Delta a_2-\varphi_2'\frac{\partial A_2^0(z,t)}{\partial z}, \tag{23}$$

$$\frac{\partial b}{\partial t}=\Delta b-A_1^0(z,t)b-B^0(z,t)a_1-\varphi_1'\frac{\partial B^0(z,t)}{\partial z},$$

$$\frac{\partial s}{\partial t}=\Delta s+A_1^0(z,t)b+B^0(z,t)a_1-\varphi_1'\frac{\partial S^0(z,t)}{\partial z},$$

$$\Delta=\frac{\partial^2}{\partial z^2}-k^2,$$

where $\varphi_i'=-Ik\varphi_i$ and with boundary conditions:

$$z\to-\infty:\quad \varphi_1=0,\quad \frac{\partial\varphi_1}{\partial z}=0,\quad \vartheta_1=0,\quad a_1=0,$$

$$b=0,\quad s=0,$$

$$z\to+\infty:\quad \varphi_2=0,\quad \frac{\partial\varphi_2}{\partial z}=0,\quad \vartheta_2=0,\quad a_2=0,$$

$$z=0:\quad \varphi_1=\varphi_2=0,\quad \frac{\partial\varphi_1}{\partial z}=\frac{\partial\varphi_2}{\partial z},$$

$$\frac{\partial^2\varphi_1}{\partial z^2}=\eta\frac{\partial^2\varphi_2}{\partial z^2}-k^2(M\vartheta_1+M_Aa_1+M_Ss),$$

$$\vartheta_1=\vartheta_2,\quad \frac{\partial\vartheta_1}{\partial z}=\kappa\frac{\partial\vartheta_2}{\partial z},\quad a_1=a_2,$$

$$\frac{\partial a_1}{\partial z}=D\frac{\partial a_2}{\partial z},\quad \frac{\partial b}{\partial z}=0,\quad \frac{\partial s}{\partial z}=0.$$

The flow equations in (23) are splitted out from the rest of the system and the equations for φ_1 and φ_2 can thus be solved independently and analytically. We get

$$\varphi_1(t,z)=\frac{\epsilon k^2}{1+\eta}(M\vartheta_1|_{z=0}+M_Aa_1|_{z=0}+M_Ss|_{z=0})\times(e^{kz}-e^{z\sqrt{k^2+1/\epsilon}}),$$

$$\varphi_2(t,z)=-\frac{\epsilon k^2}{1+\eta}(M\vartheta_1|_{z=0}+M_Aa_1|_{z=0}+M_Ss|_{z=0})\times(e^{-kz}-e^{-z\sqrt{k^2+1/\epsilon}}). \tag{24}$$

There are two methods commonly used to determine the stability of a time-dependent flow: (a) the quasisteady-state approximation (QSSA), in which we freeze the time and determine the growth constant as if the base state is steady; and (b) the solution of the initial value problem (IVP) for small disturbances. The first method neglects the rate of change of the base state and leads to an eigenvalue problem with time appearing as a parameter. The second method is an exact solution for the initial value problem, which brings the initial data into consideration. Tan and Homsy have shown for viscous fingering problems in Ref. 27 that the initial value calculation gives essentially the same results as the quasisteady-state approach, except for a short period of time in which the base state changes rapidly. In our case the system becomes unstable only after some critical period of time. Therefore it is reasonable for us to use the method of initial value calculations.

Thus, in order to find stability conditions, Eqs. (23) and (24) are numerically integrated together with the equations for the base state (21) to compute the growth rate λ for a given wave number k. Repeating the calculations for varying k enables us to describe the growth of small disturbances over a range of wave numbers. As is known, the growth rate for time-dependent stability problems is both time and space dependent and is no longer uniquely defined. However, we find, like previous authors,[27] that choosing different definitions of the growth rate does not affect the character of the solutions. We present here stability results obtained by initial value calculations of the growth rate λ defined similarly to a Lyapunov exponent:

$$\lambda(t)=\frac{1}{N}\sum_{j=1}^{N}\frac{1}{\Delta t}\ln\frac{a_{1j}(t+\Delta t)}{a_{1j}(t)}, \tag{25}$$

where Δt is the integration time step and N is the number of independent realizations (typically N is equal to 10–15). Because the growth rate λ is sensitive to the given initial data, each independent integration starts from white noise with an amplitude less than 10^{-4}. We have fixed the occurrence of instability to the time when $\lambda(t)$ averaged over several realizations changes sign from negative to positive.

The typical growth rate of flow perturbation plotted versus time for the particular case $\gamma=1$, $\mathrm{Bi}=\infty$, $M=30000$, $k=0.4$ is shown as the inset to Fig. 5(a). One can see that no unusual growth, which is so characteristic for nonmodal resonance phenomena [Trefethen *et al.*[28]], occurs at the beginning, which implies that no pseudomodes exist there. When the reaction just starts, the system is stable, all perturbations decay. The growth becomes positive at about $t\approx2.5$, and again negative at $t\approx6.5$. The nature of this growth is quite simple and is related with Marangoni instability (will be discussed below in more detail).[29–31] Let us discuss now the results we have obtained for different sources of instability.

B. Pure thermal instability

To begin, let us determine the sensitivity of the system to a Marangoni instability of pure thermal nature, when $M_A=0$ and $M_S=0$. Two different cases will be considered: the first one is the case of highly conductive sidewalls $\mathrm{Bi}=\infty$ and the second one is the case of perfect thermal insulators $\mathrm{Bi}=0$. Neutral curves for the former case are plotted in the plane time versus wave number in Figs. 5(a) and 5(b) for both $\gamma=1$ and $\gamma=10$, respectively (note that instability occurs inside the balloons). One can see that the critical wavelength of the convective pattern does not depend practically on variation of γ. In both cases the instability pattern starts

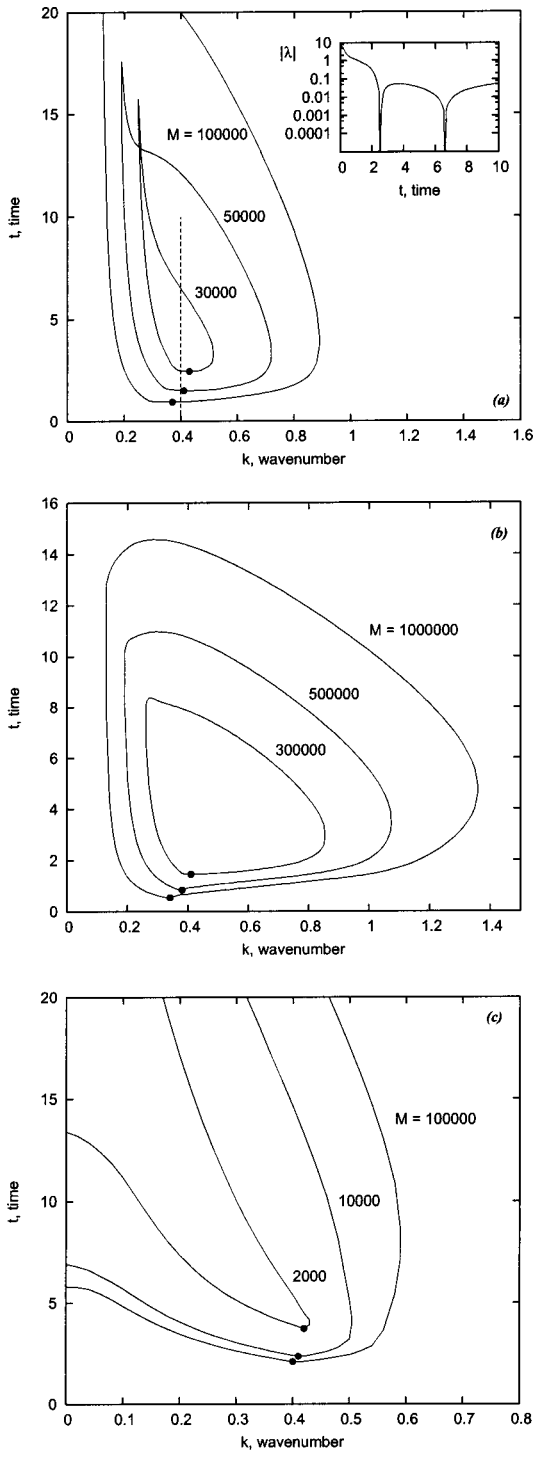

FIG. 5. Neutral curves for pure thermal Marangoni instability for Bi$=\infty$ [(a), (b)] and Bi$=0$ (c) for $\gamma=1$ [(a), (c)] and $\gamma=10$ (b). The variation of the absolute value of growth rate λ versus time for the case $M=30\,000$, $k=0.4$ is shown in a logarithmic scale in the inset to (a) (the corresponding cross section in the figure itself is plotted as a dashed line).

from $k\approx 0.4$ and arises at about $t\approx 1$. But as for other features, Figs. 5(a) and 5(b) show rather different behavior of the system. The main difference is that the thermally-driven instability is more easily triggered in the case of equal initial concentrations of acid and base. Indeed for $\gamma=1$, convection may already occur at $M=2.5\cdot 10^4$ [Fig. 5(a)] while in the case $\gamma=10$ it happens only at $M=1.4\cdot 10^5$ [Fig. 5(b)]. It means that for a given system with some fixed reactants, a decrease of the initial base concentration stabilizes the system with respect to a thermally-driven Marangoni instability.

In fact, this result might have been expected from the base state calculations presented in the previous section. Indeed, when the initial concentration of acid is higher than that of the base and $\gamma>1$, a part of the acid cannot find base to produce salt. The total heat release therefore decreases, which manifests itself [see Fig. 3(b)] by a decrease of the temperature gradient at the interface (which can be treated as a local heat Marangoni number).

Another effect seen in Fig. 5, comparing pictures a and b, is that the instability at $\gamma=1$ lasts longer: if one may expect at $\gamma=1$ the instability in the time range $1<t<100$ (for $M=3\cdot 10^5$), the same system at $\gamma=10$ is unstable only in the range $2<t<8$. The explanation for that is also straightforward: when initial concentrations of reactants are equal, the reaction front stays in a quasisteady position near the interface [see Fig. 2(b)], and most of the heat releases there. For $\gamma>1$, the reaction front begins to move faraway from the interface at about $t\approx 6$ [see Fig. 3(b)]. The temperature maximum follows this movement weakening the heat Marangoni effect at the interface.

Now let us see what happens when Bi$=0$. Neutral curves for this case are plotted in Fig. 5(c) for $\gamma=1$. One can notice the important difference with the previous case: when time exceeds some critical value, the long-wave mode $k=0$ becomes unstable as well. By varying the Marangoni number M and parameter γ, we find nevertheless that long-wave instability never happens first, i.e., the primary instability is always short-wave.

C. Pure solutal instability

Let us now turn to the pure solutal instability, when $M=0$. There are two cases which are interesting: the Marangoni effect driven only by salt $M_A=0$ and the same effect driven only by acid $M_S=0$.

Neutral curves for solutal Marangoni instability due to salt are presented in Figs. 6(a) and 6(b), where a and b refer to the cases $\gamma=1$ and $\gamma=10$, respectively. We see that the salt produces a Marangoni instability with a higher wave number compared to the thermal instability. As for other features, the situation is the same as in the previous case: the instability starts at about $t\approx 1$, i.e., the disturbances need a similar time to grow. The most intensive and long lasting instability arises for $\gamma=1$ [Fig. 6(a)] rather than for $\gamma=10$ [Fig. 6(b)]. In the first case, $M_S\approx -40$ is sufficient to induce convection. The explanation is the same as above: as the salt is the product of reaction, a higher concentration of salt is produced if the initial concentrations of acid and base are equal. It is remarkable that the critical values of the solutal Marangoni number M_S, at which instability can occur for the cases $\gamma=1$ and $\gamma=10$ differ approximately by a factor of 10, i.e., exactly the same ratio as γ. Thus, we can conclude that increasing γ results in a system which is more stable with regard to thermal and salt-driven solutal Marangoni instabilities.

Let us discuss now what happens when the Marangoni

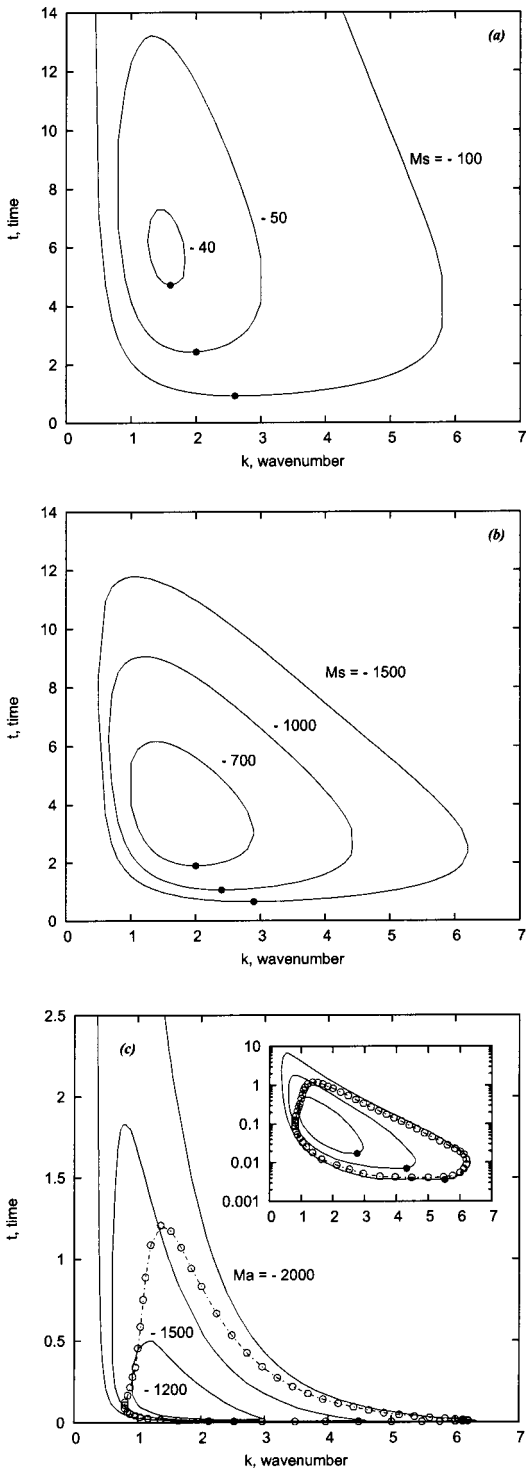

FIG. 6. Neutral curves for pure solutal Marangoni instability induced by salt for $\gamma=1$ (a) and $\gamma=10$ (b). Curves for pure acid-driven solutal Marangoni instability is shown in (c), where results for $\gamma=1$ and $\gamma=10$ are indicated by dotted (only for $M_A=-2000$) and solid lines, respectively. To clarify the process at early time, the curves are also presented in a logarithmic scale in the inset.

effect is driven only by acid. Figure 6(c) summarizes all results concerning the role of acid. The acid-driven instability has features which are qualitatively different from the cases discussed above. The instability due to the interfacial effect of acid starts from the very beginning, already at about $t\approx 5\cdot 10^{-3}$ (for $M_A=-2000$). This fact can be explained by the higher concentration of acid present from the very beginning of the process. In contrast, the temperature and the salt concentration as products of the reaction need some time (about 1 unit of time) to grow from zero up to an amount above which instability becomes possible.

The wave number of the pattern at onset strongly depends on the solutal Marangoni number M_A. The critical wave number tends to infinity $k_{\mathrm{cr}}\to\infty$ as the Marangoni number grows to $M_A\to-\infty$. Hence, for very high Marangoni numbers the wavelength of the pattern eventually becomes smaller than the Hele-Shaw gap width making the Hele-Shaw approximation senseless. The estimation of the largest possible wave number compatible with our Hele-Shaw model gives the value $k^*\approx 6$. The neutral curves show that the wave number of the pattern tends to zero ($k_{\mathrm{cr}}\to 0$) as time goes by. The instability induced by acid is comparatively short-living with regard to that induced by salt. For example, for $M_A=-1200$ the system becomes stable with respect to acid-driven disturbances already after $t\approx 0.5$ [Fig. 6(c)].

We can see from Fig. 6(c), that the parameter γ has on the instability induced by acid an effect reverse to that induced by salt: increasing γ destabilizes the system with regard to the acid as the most intensive consumption of acid occurs if $\gamma\to 1$ for which the interfacial effect of acid decreases.

Let us note that the Marangoni instability induced by the acid may be qualitatively described as follows: a disturbance that increases the interfacial concentration of the acid, such as fluid from the bulk of the upper layer reaching the interface, will produce a local increase ($\partial\sigma/\partial A>0$) in interfacial tension leading to attracting movements. In the bulk, these movements penetrate deeper in the phase of higher viscosity, i.e., in the lower layer. Thus fluid from the upper layer replacing the displaced interfacial elements will come from an area closer to the interface than the fluid from the lower layer. Finally, transfer of the acid through the interface during flow along the interface will cause an increase in the interfacial concentration maintaining the surface tension gradient. As a result, the system will be unstable. This picture looks like the instability induced by the solute diffusing from a phase A to a phase B with parameters $D_A/D_B>1$, $\nu_A/\nu_B<1$ discussed in the article by Sternling and Scriven,[14] who predicted a stationary cellular instability for that case. It should be noted, however, that such qualitative consideration must be conducted very carefully when chemical reactions take place close to the interfacial region.

Another complexity originates from the following fact. Sternling and Scriven[14] have considered the system with fixed gradients of concentration near the interface. In our case, the gradients of all quantities are transient. This turns the steady pattern into a dynamical one developing in time. There are two mechanisms competing here: first the gradient G of concentration (or of heat) near the interface and second the characteristic size D of instability zone. Both quantities are included in a local Marangoni number which can be written as $M_{\mathrm{loc}}(t)=\alpha G(t)D^2(t)$ (α is some time-independent coefficient). At the beginning of the process [see Fig. 2(a),

acid profile in the base state], the gradient of acid near the interface is large, but the instability zone (the range where acid concentration is nonuniform) is close to zero. As a result, we have a small $M_{\mathrm{loc}}(t)$ and stability of the system—this is why all disturbances decay at the start. As time goes by, the acid gradient G decreases due to diffusion, but the characteristic size D grows much faster. As a consequence $M_{\mathrm{loc}}(t)$ also grows and finally exceeds some critical value. As a result, the convection starts. Note that, in the course of time, when D grows steadily, the wavelength of the pattern also increases monotonically. This is why we observe the pattern with growing wavelength described in the paper.

Summarizing our findings, we can conclude that in the range $0<t<1$ the destabilizing effect of acid is dominant. At later stage this effect decreases, while heat and salt-driven Marangoni effects become then more important for the system.

D. Mixed-mode instability

To conclude the discussion on linear stability, let us give some examples of mixed-mode instability, when two or even all three possible mechanisms, which were described above, act simultaneously in the system. Figure 7 shows how complicated the coupling of different modes may be even within the linear analysis. Neutral curves in the case where both thermal and acid-driven solutal effects are present are shown in Fig. 7(a) for $\gamma=10$. One can see that even a weak production of heat can have a strong effect on the solutal instability induced by acid: increasing the thermal Marangoni number leads to a more stable system with smaller wave numbers. Figure 7(b) shows the joined action of the two solutal modes: both effects help each other resulting in a wider instability balloon. And, at last, the interesting coupling of all three modes of instability is shown in Fig. 7(c). It turns out that a sufficiently strong dependence of surface tension on temperature can fully protect the system from the instability induced by acid at earlier times.

As already noted by Ibanez and Velarde,[32] it is of interest to mention the relative role of reaction (R), diffusion (D), and convection (C). Whereas each pair of them leads to either full stability (RD, RC) or short living weak instability (DC), all together the three mechanisms produce a much stronger effect leading to reaction-diffusion-convection patterns.

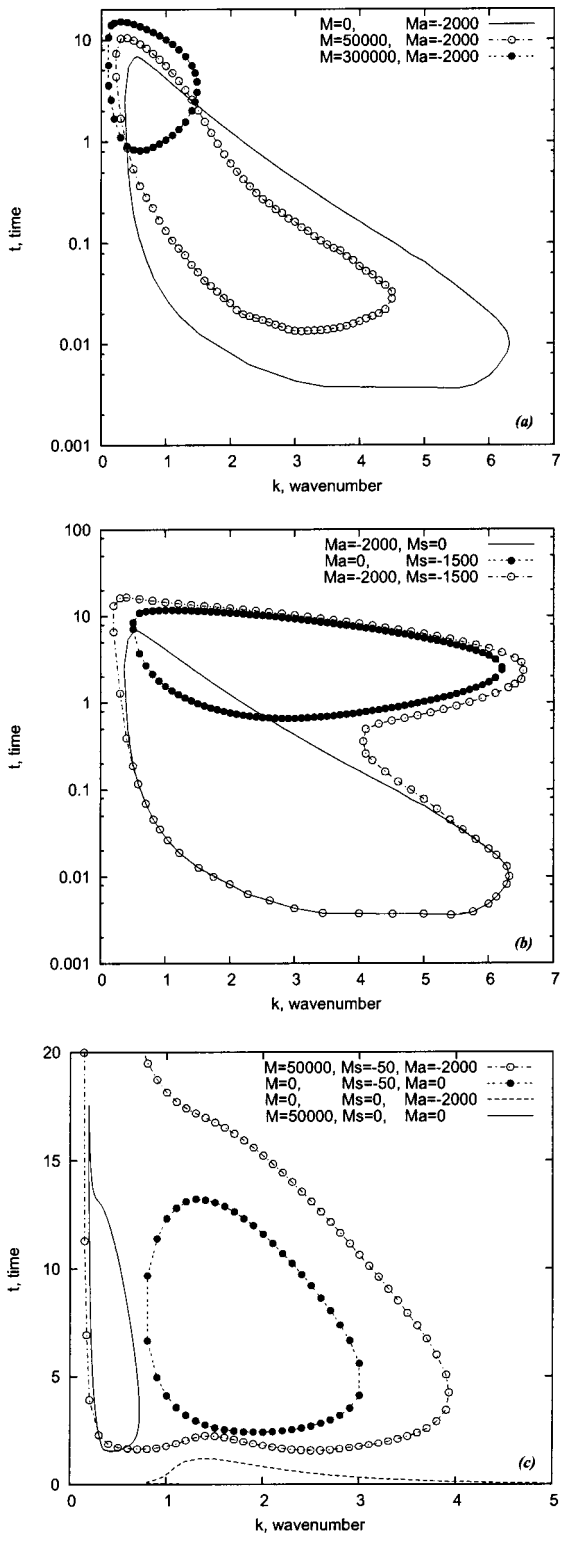

FIG. 7. Neutral curves for mixed-mode instabilities: (a) thermal-solutal (acid) two-mode instability for $\gamma=10$, (b) solutal acid-salt two-mode instability for $\gamma=10$, (c) thermal-solutal acid/salt three-mode instability for $\gamma=1$.

V. NONLINEAR DYNAMICS

A. The solution method

In order to perform nonlinear simulations of the two-dimensional system, we use the vorticity-stream function formulation of the governing Eqs. (20), where the vorticity is defined as

$$\Phi_i=-\Delta\Psi_i.$$

We solve the system of equations in the domain $0<x<H$, $-L<z<L$ with $z=0$ being the interface between the upper and lower layers. No-slip boundary conditions for the velocities and the requirement that the normal derivatives of the temperature and concentrations vanish are applied at the horizontal boundaries:

$$z=-L:\quad \Psi_1=0,\quad \frac{\partial\Psi_1}{\partial z}=0,\quad \frac{\partial T_1}{\partial z}=0,$$

$$\frac{\partial A_1}{\partial z}=0,\quad \frac{\partial B}{\partial z}=0,\quad \frac{\partial S}{\partial z}=0,$$

$$z=-L:\quad \Psi_2=0,\quad \frac{\partial\Psi_2}{\partial z}=0,\quad \frac{\partial T_2}{\partial z}=0,\quad \frac{\partial A_2}{\partial z}=0.$$

At the vertical boundaries we apply periodic boundary conditions. At the interface the normal components of the velocity vanish and the continuity conditions for tangential components of velocity and viscous stresses, temperatures, heat fluxes and species concentrations also apply:

$$z=0:\quad T_1=T_2,\quad A_1=A_2,\quad \frac{\partial T_1}{\partial z}=\kappa\frac{\partial T_2}{\partial z},$$

$$\frac{\partial A_1}{\partial z}=D\frac{\partial A_2}{\partial z},\quad \frac{\partial B}{\partial z}=0,\quad \frac{\partial S}{\partial z}=0,$$

$$\Psi_1=0,\quad \Psi_2=0,\quad \frac{\partial\Psi_1}{\partial z}=\frac{\partial\Psi_2}{\partial z},$$

$$\Phi_1=\eta\Phi_2+M\frac{\partial T_1}{\partial x}+M_A\frac{\partial A_1}{\partial x}+M_S\frac{\partial S}{\partial x}.$$

As the initial state we use

$$t=0:\quad \Psi_i=0,\quad T_i=0,\quad A_1=0,\quad A_2=1,$$

$$B=\frac{1}{\gamma},\quad S=0,\quad i=1,2$$

and a vorticity field characterized by one or more small one-vortex structures of intensity $\Phi\approx 10^{-3}$ located randomly close to the interface in each layer. We have checked in all cases the independence of our results on the initial condition.

The described boundary value problem is solved by finite difference methods. Equations and boundary conditions are approximated on a uniform mesh using a second order approximation for the spatial coordinates. The nonlinear equations are solved using an explicit scheme on a rectangular uniform mesh. For example, for $H=6$, $L=2$ a uniform 240×160 mesh is used. In order to ensure the stability of the numerical scheme, the time step was calculated by the formula

$$\Delta t=\frac{\Delta x^2}{2(2+\max(|\Psi_i|,|\Phi_i|))}.$$

The Poisson equations are solved by the iterative Liebman successive over-relaxation method in each time step: the accuracy of the solution is fixed to 10^{-4}. The Kuskova and Chudov formulas,[33] providing second order accuracy, are used for the evaluation of the vorticities at the horizontal boundaries $x=\pm L$ considered as solid:

$$\Phi_1(x,-L)=\frac{1}{2\Delta z}(\Psi_1(x,-L+2\Delta z)-8\Psi_1(x,-L+\Delta x)),$$

$$\Phi_2(x,L)=\frac{1}{2\Delta z}(\Psi_2(x,L-2\Delta z)-8\Psi_2(x,L-\Delta x)).$$

At the interface the expression for the vorticity is approximated with second-order accuracy for spatial coordinates by the formula:

$$\Phi_2(x,0)=-\frac{2(\Psi_1(x,-\Delta z)+\Psi_2(x,\Delta z))}{\Delta z^2(1+\eta)}-\frac{M}{1+\eta}\frac{\partial T_1}{\partial x}(x,0)-\frac{M_A}{1+\eta}\frac{\partial A_1}{\partial x}(x,0)-\frac{M_S}{1+\eta}\frac{\partial S}{\partial x}(x,0),$$

$$\Phi_1(x,0)=\eta\Phi_2(x,0)+M\frac{\partial T_1}{\partial x}(x,0)+M_A\frac{\partial A_1}{\partial x}(x,0)+M_S\frac{\partial S}{\partial x}(x,0).$$

Here Δx, Δz are the mesh sizes for the corresponding coordinates. The temperature and acid concentration at the interface are calculated by the second-order approximation formula:

$$T_1(x,0)=T_2(x,0)=\frac{4T_1(x,-\Delta z)-T_1(x,-2\Delta z)+\kappa(4T_2(x,\Delta z)-T_2(x,2\Delta z))}{3(1+\kappa)},$$

$$A_1(x,0)=A_2(x,0)=\frac{4A_1(x,-\Delta z)-A_1(x,-2\Delta z)+D(4A_2(x,\Delta z)-A_2(x,2\Delta z))}{3(1+D)}.$$

The numerical scheme we use is similar to a scheme proposed in Ref. 33, but generalizes it by considering additional concentration fields for the reacting chemical species. To test both accuracy and convergence of our program we have performed calculations of pure thermo-capillary convection in two-layer systems with non-vanishing gravity and without gravity recovering results reported by Liu *et al.*[34] Our code was also successfully tested and compared with results by Nepomnyashchy and Simanovskii[24] for two-layer systems with heat release at the interface. In addition, the code recovers known dynamics of the simple reaction-diffusion system.

B. Numerical results

In this section we present the results of the numerical solution of Eqs. (20) subjected to the boundary and initial conditions described in the previous section. The parameters are those for a system consisting in cyclohexane and water with following values of parameters: $\eta=0.4996$, $\kappa=0.2482$, $D=2.807$, $\mathrm{Bi}=\infty$, and $\epsilon=0.1$. All other parameters such as γ, the set of Marangoni numbers and the parameters of domain geometry H, L have been varied during the simulations.

As it was shown in the previous section, at the beginning the Marangoni instability driven by acid is leading, but as time goes by, the instabilities induced by salt and heat, products of the reaction, become more and more important. In order to show how they affect the nonlinear properties of the system, two cases are considered. First of all, we present the results of simulations when only the acid A has an interfacial effect destabilizing the system. Next, we see what happens if both the salt S and the acid A are surface active resulting in a mixed-mode instability.

First, we consider the values of parameters: $M=0$, $M_A=-2000$, $M_S=0$, and $\gamma=10$. The domain of calculation $(H=6, L=2)$ is chosen to be long in the x-direction in order to trace the dynamics of initial disturbances in more detail up to long-wave patterns $(k_{\mathrm{lim}}\approx 1)$.

Figure 8(a) shows the time dependence of the wave number of the pattern versus time computed from the nonlinear simulations and compared to the results of the linear stability analysis. Because of the dynamical character of the process, we plot here the wave number of the leading vortex. The variation with time of the stream function maximum is shown in Fig. 8(b) where the inset is a zoom on the beginning of the evolution.

The intensity of the convective flow first increases reaching its maximum at about $t=0.8$, and then slowly decreases up to zero. The initial disturbances decrease slowly up to $t\approx 0.006$, and after that they start to grow [Fig. 8(b)]. This scenario is in good agreement with the linear analysis which gives a similar value for instability onset. Figure 8(a) shows that the wave number of the pattern is located within the balloon of instability predicted by linear analysis except at the very beginning of process. As time goes by, the wavelength grows up to $k_{\mathrm{lim}}\approx 1$ at $t=1.4$, which is the limit fixed by the geometry of the numerical realization.

The acid penetrating the lower layer through the interface and producing a solutal Marangoni effect at the interface causes a permanent increase of the wavelength of the pattern through disappearance of weaker vortexes and growth of more vigorous ones. The Marangoni driven convective instability leads to a distortion of the reaction front. At the beginning, the acid penetrates in the lower layer through the whole liquid–liquid interface because of diffusion. Later on, after convection has started, the acid fluxes are concentrated only in locations periodically distributed along the interface where the higher acid concentration intensifies the solutal Marangoni effect (the fluid tends to move towards places with high concentration of acid), and amplifies the instability. As the income of fresh acid goes on, the reaction front begins to propagate slowly downwards far away from the interface. As this happens, the Marangoni effect is weakened and finally disappears. This results in the weakening of the convective pattern located near the interface and its full disappearance at time $t\approx 10$. The system then returns to its initial state, i.e., the one-dimensional reaction-diffusion state.

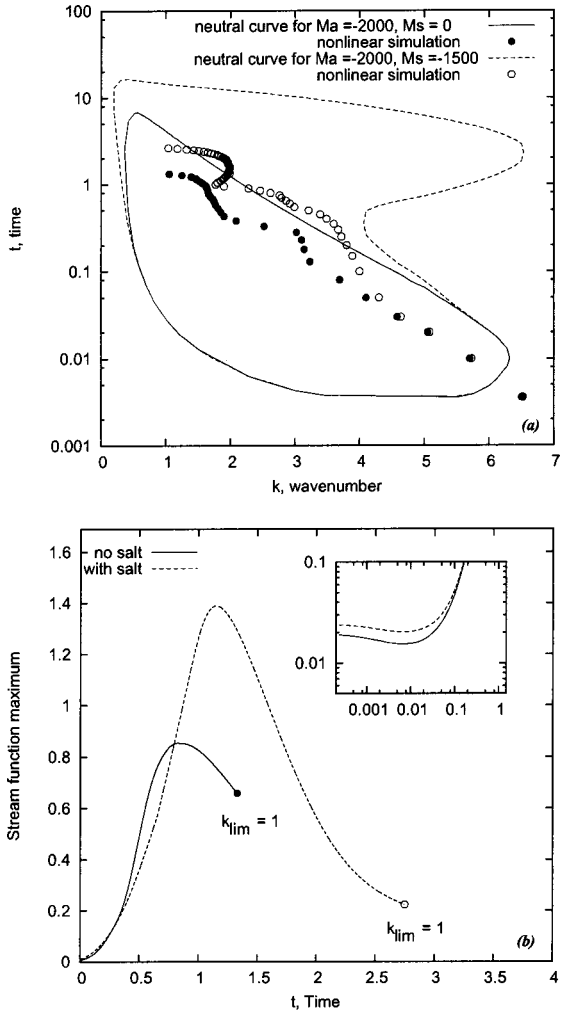

FIG. 8. Nonlinear simulation for $\gamma=10$: wavelength selection (a) and evolution of stream function maximum (b). The inset in (b) is a zoom on the evolution at early time.

Let us now concentrate our attention on the effect of salt production during the reaction. If the product of reaction, salt, was previously assumed not to be surface active, now it can influence the system dynamics through the Marangoni mechanism. This influence is governed by the solutal Marangoni number M_S. We assume also that the salt cannot cross the interface and can evolve solely in the lower layer. In order to feel the difference with the previous case, we keep all the values of parameters as before, and fix now the salt Marangoni number to $M_S=-1500$. We find [see Figs. 8(a) and 8(b)] that the salt does not change the general evolution of the system: as before, the system evolves from a short-wave pattern to a much longer structure through the permanent growth of the most vigorous vortexes. The computed streamlines (left), density plots for acid (center) and

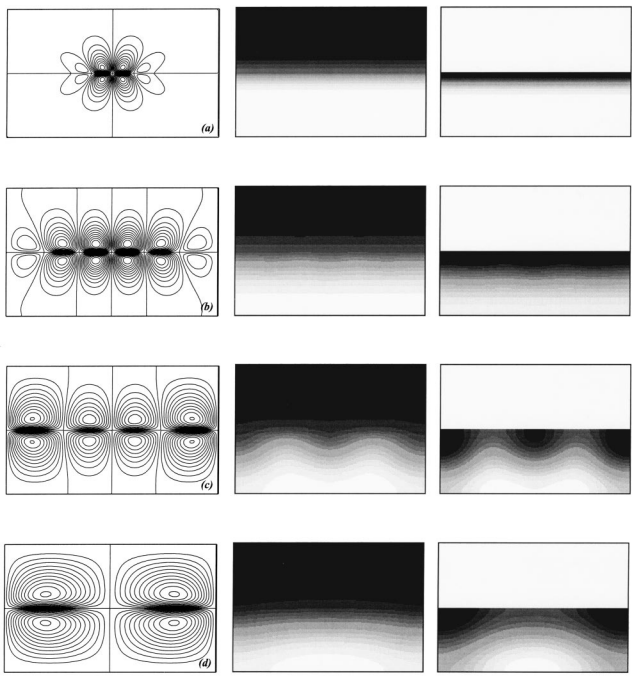

FIG. 9. Evolution of the stream function (left), density plots of acid (center) and salt (right) concentration from an initially perturbed base state to a convective pattern for $M_A=-2000$, $M_S=-1500$, $\gamma=10$. White and black in the density plot correspond to zero and maximal concentration, respectively. The frames (a), (b), (c), (d) pertain to times $t=0.0036$, 0.4, 1.5, 2.7, respectively.

salt (right) concentration for successive times are presented in Fig. 9. By taking into account the conservation law (19), the last column in Fig. 9 may be also interpreted as the density plot for the distribution of the base.

Nevertheless, the salt slightly modifies the system dynamics. First of all, the Marangoni effect produced by salt intensifies the process [Fig. 8(b)], because the interfacial tension gradients become larger (the distribution of salt in the lower layer follows the distribution of acid, and the Marangoni effects produced by acid and salt have the same sign). As a result of the resulting more vigorous fluid movement along the interface, the width of locations where acid enters the lower layer becomes narrower, and the transition of convective pattern towards larger wavelength slows down [Fig. 8(a)]. The final stage of the system evolution is similar to that without salt production.

We found also that the heat effect does not change qualitatively the described scenario, but rather accelerates the system evolution to patterns with a longer wavelength, since the thermal Marangoni instability occurs at smaller wave numbers than the solutal one.

VI. DISCUSSION AND CONCLUSIONS

The main objective of this article is to highlight the role of Marangoni instabilities in pattern formation observed when chemical reactions are at play close to the interface between two immiscible fluids.

We have shown that Marangoni patterns may arise as a result of a complicated interplay between diffusion, chemical reactions giving rise to heat release and convection in the bulk close to the interface. Let us describe this process in detail. An important role in the occurrence of the instability is played by the diffusion of one of the reactant, acid *A*, from one layer to the other. This gives the onset of the exothermic chemical reaction in the fluid below the interface where the acid meets a base *B* to provide a salt *S* in a neutralization reaction. When the acid crosses the liquid–liquid interface, it immediately gives rise to solutal Marangoni convection characterized at early times by a short-wave pattern if the acid is surface active.

As the system evolves in time, the products of the reaction, heat and salt, become increasingly important for the system stability when their amount reaches the level above which thermal and salt-driven Marangoni effects come into play. Finally, the system is self-organized as follows: convection brings fresh reactant from the upper layer to the lower one intensifying mass transfer in the system. This speeds up the reaction and raises the heat release leading to a self sustained chemo-hydrodynamic pattern.

Nevertheless, the resulting pattern can exist only during a finite time as the underlying reaction-diffusion base state is not steady. As time goes by, the reaction front travels far away from the interface. The convection driven solely by Marangoni mechanisms can not be further supported and decays eventually. Hydrodynamical instabilities could be further sustained only if gravity could come into play allowing for new mechanisms such as Rayleigh–Bénard or double diffusion ones to relay Marangoni effects.

Let us finally estimate the critical values for the Marangoni numbers, for example, for the system experimentally studied in Ref. 11 in order to be sure that the instability considered in the present paper is realistic. Taking into account that the value for the change of the surface tension of water with the salt concentration $\sigma_S=0.51\times10^{-3}$ N/(m∗mol/l) and other physical characteristics are $Q=-5$, 7×10^4 J/mol, $A_0\approx0.1$ mol/l, $\kappa_1=0.6$ W/(m∗K), $D_{A1}=10^{-9}$ m^2/s, $\eta_1=10^{-3}$ Pa∗s, $h\sim10^{-3}$ m, the solutal Marangoni number due to salt may be estimated as $M_S\sim-10^4$. For the thermal Marangoni number we obtain $M\sim10^4$. By comparing these values with those presented in Figs. 5 and 6, we see that the discussed system is more sensible to the solutal Marangoni effect than to thermal one, but anyway the thermal Marangoni instability can also occur. All the critical conditions of the instability correspond to physically realistic values of parameters. The wavelength of the resulting pattern at onset is approximately equal to 2–3 times the gap-width of the Hele-Shaw cell, i.e., 2–3 mm followed by increase of its size in time. The averaged total lifetime is about 10–20 min (1–2 units of dimensionless time). The described pattern formation should therefore be observed experimentally either in horizontal Hele-Shaw cells on Earth or ideally in zero-gravity.

ACKNOWLEDGMENTS

We wish to thank K. Eckert, M. Acker, and Y. Shi for stimulating discussions and for sharing their experimental results with us prior to publication. Discussions with G. M.

Homsy, A. A. Nepomnyashchy, and H. Dijkstra are acknowledged. This work is financially supported by Prodex [Contract No. 14556/00/NL/SFe(IC)] and ESA (Contract No. 15196/01/NL/SH). A.D. is a Research Associate at the FNRS (Belgium). D.B. wishes to thank the Office for Scientific, Technical, and Cultural Affairs (Belgium) for their financial support.

[1] A. A. Nepomnyashchy, M. G. Velarde, and P. Colinet, *Interfacial Phenomena and Convection* (Chapman and Hall/CRC, Boca Raton, 2002).
[2] G. Quincke, ''Ueber periodische Ausbreitung an Flussigkeitsoberflachen und dadurch hervorgerufene Bewegungserscheinungen,'' Ann. Phys. (Leipzig) **35**, 580 (1888).
[3] T. S. Sherwood and J. C. Wei, ''Interfacial phenomena in liquid extraction,'' Ind. Eng. Chem. **49**, 1030 (1957).
[4] M. Dupeyrat and E. Nakache, ''Direct conversion of chemical energy into mechanical energy at an oil–water interface,'' Bioelectrochem. Bioenerg. **5**, 134 (1978).
[5] E. Nakache, M. Dupeyrat, and M. Vignes-Adler, ''Experimental and theoretical study of an interfacial instability at some oil–water interfaces involving a surface-active agent,'' J. Colloid Interface Sci. **94**, 187 (1983).
[6] E. Nakache and M. Dupeyrat, ''The contribution of chemistry to new Marangoni mass transfer instabilities at the oil/water interface,'' Faraday Discuss. Chem. Soc. **77**, 189 (1984).
[7] *Science and Practice of Liquid–Liquid Extraction*, edited by J. D. Thornton (Clarendon, Oxford, 1992).
[8] D. Avnir and M. L. Kagan, ''The evolution of chemical patterns in reactive liquids driven by hydrodynamic instabilities,'' Chaos **5**, 589 (1995).
[9] S. Kai, S. C. Müller, T. Mori, and M. Miki, ''Chemically driven nonlinear waves and oscillations at an oil–water interface,'' Physica D **50**, 412 (1991).
[10] K. Eckert and A. Grahn, ''Plume and finger regimes driven by a exothermic interfacial reaction,'' Phys. Rev. Lett. **82**, 4436 (1999).
[11] K. Eckert, M. Acker, and Y. Shi, ''Chemical pattern formation driven by a neutralization reaction. I. Mechanism and basic features,'' Phys. Fluids **16**, 385 (2004).
[12] S. A. Ermakov, A. A. Ermakov, O. N. Chupakhin, and D. V. Vaissov, ''Mass transfer with chemical reaction in conditions of spontaneous interfacial convection in processes of liquid extraction,'' Chem. Eng. J. **84**, 321 (2001).
[13] E. Ruckenstein and C. Berbente, ''The occurrence of interfacial turbulence in the case of diffusion accompanied by chemical reaction,'' Chem. Eng. Sci. **19**, 329 (1964).
[14] C. V. Sternling and L. E. Scriven, ''Interfacial turbulence: Hydrodynamic instability and the Marangoni effect,'' AIChE J. **5**, 514 (1959).
[15] A. Steinchen and A. Sanfeld, ''Chemical and hydrodynamic stability of an interface with an autocatalytic reaction,'' Chem. Phys. **1**, 156 (1973).
[16] A. Sanfeld and A. Steinchen, ''Coupling between a transconformation surface reaction and hydrodynamic motion,'' Biophys. Chem. **3**, 99 (1975).
[17] M. Hennenberg, T. S. Sorensen, A. Steinchen-Sanfeld, and A. Sanfeld, ''Stabilité mécanique et chimique d'une interface plane,'' J. Chim. Phys. Phys.-Chim. Biol. **72**, 1202 (1975).
[18] M. A. Mendez-Tatsis and E. S. Perez De Ortiz, ''Marangoni instabilities in systems with an interfacial chemical reaction,'' Chem. Eng. Sci. **51**, 3755 (1996).
[19] R. Texier-Picard, J. A. Pojman, and V. A. Volpert, ''Effect of interfacial tension on propagating polymerization fronts,'' Chaos **10**, 224 (2000).
[20] Yu. A. Buyevich, L. M. Rabinovich, and A. V. Vyazmin, ''Chemo-Marangoni convection. II. Nonlinear stability analysis,'' J. Colloid Interface Sci. **157**, 211 (1993).
[21] Yu. A. Buyevich, L. M. Rabinovich, and A. V. Vyazmin, ''Chemo-Marangoni convection: III. Pattern parameters: Interface mass transfer,'' J. Colloid Interface Sci. **173**, 1 (1995).
[22] M. G. Velarde, ''Drops, liquid layers, and the Marangoni effect,'' Philos. Trans. R. Soc. London, Ser. A **356**, 829 (1998).
[23] E. F. Skurygin and V. V. Dilman, ''On Marangoni instability during desorption accompanied by evaporation,'' J. Food. Eng. **43**, 125 (2000).
[24] A. A. Nepomnyashchy and I. B. Simanovskii, ''Nonlinear investigation of anticonvection and Rayleigh–Bénard convection in systems with heat release at the interface,'' Eur. J. Mech. B/Fluids **20**, 75 (2001).
[25] G. K. Batchelor, *An Introduction to Fluid Dynamics* (Cambridge University Press, Cambridge, 1967).
[26] W. Boos and A. Thess, ''Thermocapillary flows in a Hele-Shaw cell,'' J. Fluid Mech. **352**, 305 (1997).
[27] C. T. Tan and G. M. Homsy, ''Stability of miscible displacements in porous media: Rectilinear flow,'' Phys. Fluids **29**, 3549 (1986).
[28] L. N. Trefethen, A. E. Trefethen, S. C. Reddy, and T. A. Driscoll, ''Hydrodynamic stability without eigenvalues,'' Science **261**, 578 (1993).
[29] J. R. A. Pearson, ''On convection cells induced by surface tension,'' J. Fluid Mech. **4**, 489 (1958).
[30] D. A. Nield, ''Surface tension and buoyancy effects in cellular convection,'' J. Fluid Mech. **19**, 341 (1964).
[31] M. F. Schatz, S. J. VanHook, J. B. Swift, W. D. McCormick, and H. L. Swinney, ''Onset of surface-tension-driven Bénard convection,'' Phys. Rev. Lett. **75**, 1938 (1995).
[32] J. L. Ibanez and M. G. Velarde, ''Hydrochemical stability of an interface between two immiscible liquids: The role of Langmuir–Hinshelwood saturation law,'' J. Phys. (France) Lett. **38**, 1479 (1977).
[33] I. B. Simanovskii and A. A. Nepomnyashchy, *Convective Instabilities in Systems with Interface* (Gordon and Breach, London, 1993).
[34] Q. S. Liu, B. Roux, and M. G. Velarde, ''Thermocapillary convection in two-layer systems,'' Int. J. Heat Mass Transfer **41**, 1499 (1998).